

Article

Tensile Load Distribution Improvement of Three-Row Riveted Lap Joint Based on Different Squeezing Displacement Combinations

Changyi Lei ^{1,2,*}, Qinggai Huang ³ and Yunbo Bi ³ 

¹ Mechanical Engineering College, Zhijiang College of Zhejiang University of Technology, Shaoxing 312030, China

² College of Mechanical Engineering and Automatic, Zhejiang Sci-Tech University, Hangzhou 310018, China

³ College of Mechanical Engineering, Zhejiang University, Hangzhou 310027, China; ywqgorgeous@163.com (Q.H.); zjubyb@zju.edu.cn (Y.B.)

* Correspondence: zzejclcy@zjtc.edu.cn; Tel.: +86-0575-8111-2564

Abstract: Many previous studies have mainly focused on the effects of riveting parameters on single-row riveted lap joints. Little attention has been paid to multi-row riveted lap joints. The outer rows of a normal multi-row riveted lap joint usually bear a larger part of the tensile load. However, none of the studies relate the phenomenon to the squeezing displacement combination of a multi-row riveted lap joint. To improve the performance of a three-row riveted lap joint, this paper aims to reveal the internal relation between tensile load distribution, structural deformation and squeezing displacement combination. Theoretical discussion, numerical simulation and an experimental test have been conducted. Four different squeezing displacement combinations have been studied. The result indicates that an appropriate squeezing displacement combination can effectively make tensile load distribution more homogeneous. Each rivet can take approximately 33% tensile load. Structural deformation magnitude can be reduced as well. Compared with the worst situation, at the region most sensitive to tensile load, the max strain value can reduce about 53.22–79.76%. A suitable squeeze displacement combination is a simple approach for the performance enhancement of a three-row riveted lap joint. It can be practically applied in aircraft manufacturing without any additional equipment or skill learning.

Keywords: three-row riveted lap joint; squeezing displacement combination; tensile load distribution; structural deformation



Citation: Lei, C.; Huang, Q.; Bi, Y. Tensile Load Distribution Improvement of Three-Row Riveted Lap Joint Based on Different Squeezing Displacement Combinations. *Coatings* **2021**, *11*, 856. <https://doi.org/10.3390/coatings11070856>

Academic Editor: Filippo Berto

Received: 16 June 2021

Accepted: 12 July 2021

Published: 16 July 2021

Publisher's Note: MDPI stays neutral with regard to jurisdictional claims in published maps and institutional affiliations.



Copyright: © 2021 by the authors. Licensee MDPI, Basel, Switzerland. This article is an open access article distributed under the terms and conditions of the Creative Commons Attribution (CC BY) license (<https://creativecommons.org/licenses/by/4.0/>).

1. Introduction

The riveted lap joint is an effective and important connection mode to permanently fasten aircraft structures. There are approximately 1,500,000–2,000,000 rivets and bolts in a modern large aircraft [1]. A representative connection mode in pressurized aircraft fuselage is the three-row riveted lap joint [2]. Figure 1 illustrates a typical fuselage longitudinal riveted lap joint. The rivets are not only used as fasteners, but also act as an indispensable medium for load transmission between different parts.

The Aloha Airlines accident in 1988 has warned aircraft manufacturers and researchers of the continuing need to improve the performance of a riveted lap joint. Many scholars have carried out detailed work to investigate the riveting parameters of a single-row rivet connection. Previous research has summarized the main structure parameters and procedure parameters of a single-row riveted lap joint [3]. However, compared with single-row riveted lap joints, fewer studies focus on multi-row riveted lap joints.

A riveted lap joint mainly bears tensile load when in flight. The tensile load is almost transmitted by rivets. Generally, the tensile load distribution among rivet rows is not homogeneous, especially when a riveted lap joint has more than two rows. The outer rows usually transfer a larger part of the tensile load than the inner rows. Inhomogeneous tensile

load transmission would make the outer rows more susceptible to fatigue damage [4,5]. Residual stress distribution after the tensile stage will be influenced as well [6]. More stress concentration regions may appear. Moreover, the high stresses around the fastener holes will affect the performance of a multi-row riveted lap joint [7,8].

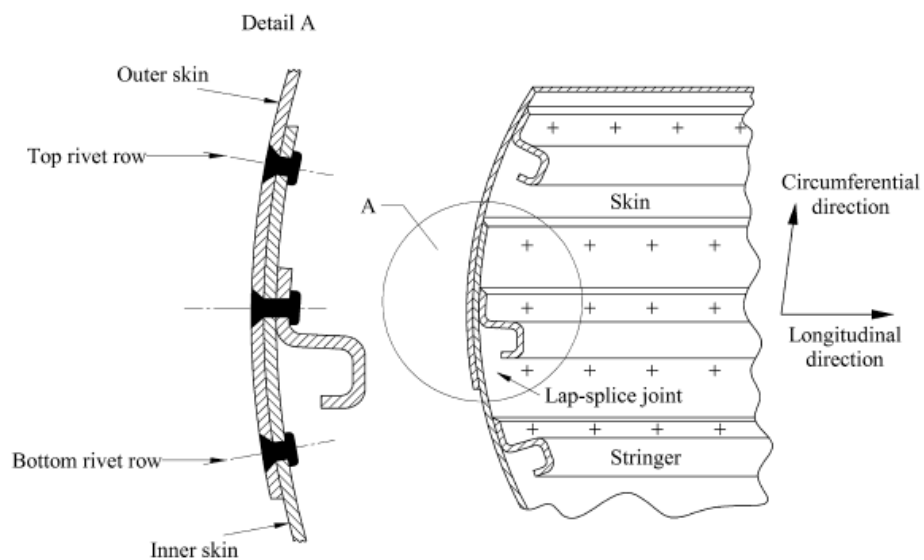


Figure 1. Typical fuselage longitudinal riveted lap joint [2] Reproduced with permission from Skorupa, A; INT. J. FATIGUE, published by Elsevier, 2014.

Aman [9] attempted to find out the effects of some controllable process parameters on the quality of a riveted lap joint. Park [10] investigated the influence of various parameters on the fatigue behavior of riveted lap joints. The relation between load transmission and the cracking behavior at countersunk fastener holes has been described. Atre and Johnson [11] established a global three-rivet model of a fuselage lap joint. The residual stresses during rivet installation and the fuselage pressurization process had been taken into account. The results showed that the effects of underdriven rivets were critical to the stress state of a fuselage splice. Jiang [12] analytically calculated the tensile load carried by each rivet based on a multi-rivet connection. Liu [13] analyzed the effect of sheet bending on load distribution among different rivets.

Structural deformation happens during riveting and the tensile process. The sheet expands in the longitudinal and transverse directions. Abdelal [14] found methods to control the dimensional growth through a series of numerical simulations and probabilistic analysis. Longitudinal and transverse deformation had significant effects on the performance of a riveted panel. Moreover, Yuan [15] conducted fastener load-transferred experiments and fatigue tests based on scarfed lap joints with different lap angles. Both the test results and predicted data showed that the fatigue life of scarfed lap riveted lap joints was remarkably increased after introducing the lap angle into the faying surface.

Among studies, little attention has been paid to analyzing the influence of different squeezing displacement combinations on tensile load transmission of a multi-row riveted lap joint.

Squeezing displacement is one of the most important riveting parameters. On the one hand, squeezing displacement can reflect the magnitude of driven head dimension after riveting. Additionally, the driven head dimension is considered as an indication of the fatigue performance of a riveted lap joint [16,17]. A larger squeezing displacement can introduce a greater residual stress around a rivet. On the other hand, compared with other process parameters, squeezing displacement is a simple and easily controllable parameter. It can be applied in aircraft manufacturing without any additional equipment.

Hence, this paper proposes the development of a deep understanding of the internal relationship between different squeezing displacement combinations, tensile load distributions and the corresponding structural deformation. The aim is to find out the appropriate squeezing displacement combination to achieve a more homogeneous tensile load distribution. The other purpose is to improve the structural deformation of a riveted lap joint simultaneously. The research in this paper is helpful in effectively improving the performance of three-row riveted lap joints.

2. Load Transmission and Structural Deformation

Secondary bending and longitudinal deformation appear when a riveted lap joint sustains a tensile load. Figure 2 illustrates the regional structure deformation of a riveted lap joint. The riveted lap joint can be considered as a symmetrical structure. The dimension and rivet hole layout of the outer sheet keep the same as the inner sheet.

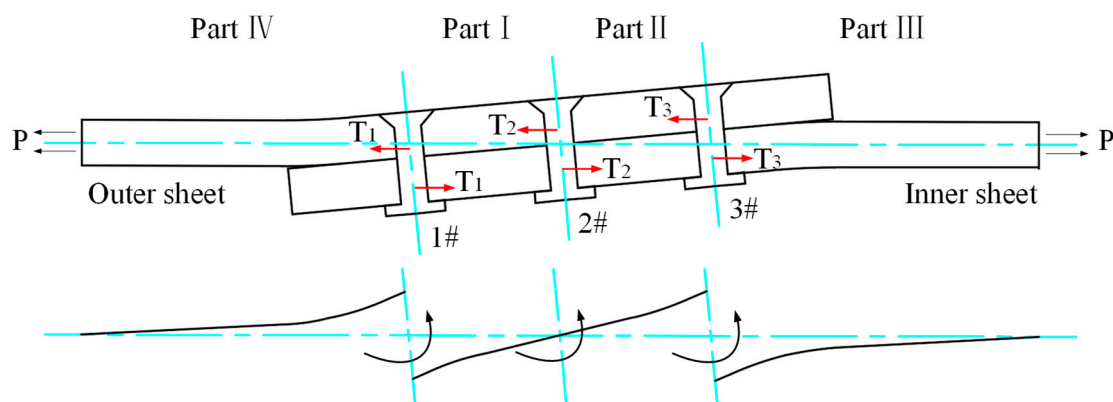


Figure 2. Regional deformation of the riveted lap joint.

In the tensile stage, the tension load is mainly transmitted by rivets 1#, 2# and 3#. The rest of the tensile load is delivered by the friction between the mating surfaces. Four parts can be divided for a three-row riveted lap joint: Part I, Part II, Part III and Part IV. For the inner sheet, the tensile load P is transferred from the outer side to Part III, and finally, to Part I. The average strains of parts I, II and III in the inner sheet are assumed to be ϵ_{i1} , ϵ_{i2} , and ϵ_{i3} . For the outer sheet, the tensile load travel path is from the outer side to Part IV, Part I and Part II. The average strains of parts I, II and IV in the outer sheet are assumed to be ϵ_{o1} , ϵ_{o2} , and ϵ_{o4} .

All rows take part in the load delivering from one sheet to the other sheet. The parts of tensile load P transmitted by the three rivets are assumed to be T_1 , T_2 , and T_3 . Because of the symmetry, $T_1 = T_3$, thus:

$$P = T_1 + T_2 + T_3 = 2T_1 + T_2 \tag{1}$$

Obviously, ϵ_{i3} and ϵ_{o4} are the total strain caused by tensile load $P = T_1 + T_2 + T_3$. ϵ_{i2} and ϵ_{o1} are the strain caused by $T_1 + T_2$. ϵ_{i1} and ϵ_{o2} are the strain caused by T_1 .

The deformation degree of the inner sheet is:

$$\epsilon_{i3} > \epsilon_{i2} > \epsilon_{i1} \tag{2}$$

Similarly, the deformation degree of the inner sheet is:

$$\epsilon_{o4} > \epsilon_{o1} > \epsilon_{o2} \tag{3}$$

Meanwhile, in Part I, $\epsilon_{o1} > \epsilon_{i1}$; in Part II, $\epsilon_{o2} < \epsilon_{i2}$.

Structural deformation is a gradual process. In the outer sheet, the maximum deformation occurs in the vicinity of Rivet 1#. The minimum deformation appears at Rivet 3#.

Conversely, in the inner sheet, the maximum deformation occurs in the vicinity of Rivet 3#. The minimum deformation appears at Rivet 1#. Therefore, the interface of Part IV and Part I in the outer sheet as well as the interface of Part II and Part III in the inner sheet are the most dangerous areas of a three-row riveted lap joint. Since the interfaces have the minimum section surface area, the interfaces suffer to the total tensile load P .

Different strain level can result in different elongations of each part, whether in the outer sheet or inner sheet. As a consequence, an internal moment will be introduced at the three fastener rows, M_1 , M_2 , and M_3 , separately. The “internal moment model” can effectively explain the relationship between tensile load distribution and structural deformation [8]. Figure 3 illustrates the internal moment model based on the three-row riveted lap joint.

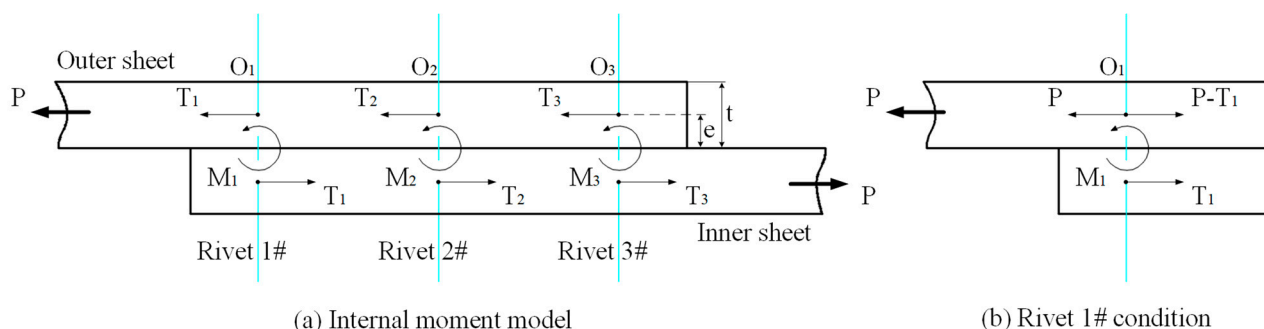


Figure 3. The internal moment model based on the three-row riveted lap joint. (a) Internal moment model. (b) Rivet 1# condition. Notes: t is the sheet thickness. e is the eccentricity.

In the model, the outer and inner sheets are subjected to secondary bending and longitudinal deformation because of the different elongations. For Rivet 1#, on the one hand, T_1 and $P - T_1$ are no longer equal according to Equation (1). On the other hand, the resultant force of tensile load transfer does not act at the neutral line of the overlap region, as shown in Figure 3b. The internal moment M_1 is introduced to account for this effect. The internal moment M_1 is closely related to the tensile load distribution and geometric dimension of the joint. For a monolithic joint, the neutral line is located at the center of the joint. $e = t/2$ is a constant. Thus, the internal moment mainly relies on tensile load distribution. The internal moment M_1 , which acts on the point O_1 of Rivet 1# in the clockwise direction, can be calculated as follows:

$$-M_1 + P_1 \times \frac{t}{2} - (P - T_1) \times \frac{t}{2} - T_1 \times \frac{3}{2}t = 0 \tag{4}$$

$$-M_1 + T_1 \times \frac{t}{2} - T_1 \times \frac{3}{2}t = 0 \tag{5}$$

$$M_1 = -T_1t \tag{6}$$

Likewise, the internal moments in the second and third rivet rows can be represented by Equations (7) and (8).

$$M_2 = -T_2t \tag{7}$$

$$M_3 = -T_3t \tag{8}$$

Obviously, tensile load distribution has a significant influence on structural deformation. Improving the distribution uniformity of the tensile load can significantly reduce the internal moment acting around Rivet 1# and Rivet 3#. The internal moments between the three rivets will become more homogenous. The gap of different elongations for each part will become smaller. The magnitude of structural deformation can be improved, especially at the outer rows. The assembly quality and fatigue performance of a three-row riveted lap joint can be greatly enhanced.

3. Materials and Methods

3.1. Materials

In this study, the material of the outer and inner sheets is 7050-T7451 Al alloy. The material of the rivet is 7075-T62 Al alloy. Ludwik's material model is employed to represent the relationship between true stress and true strain. Table 1 lists the material properties [18]. An isotropic hardening behavior is assumed for the materials of sheets and rivets. In Table 1 and Equation (9), ε is the true strain and $\sigma(\varepsilon)$ is the true stress. A and B are material constants. n describes the hardening behavior.

$$\sigma(\varepsilon) = A + B \times \varepsilon^n \quad (9)$$

Table 1. Elastic and Plastic Properties for Sheet and Rivet Materials.

Type	E/GPa	ν	A/GPa	B/GPa	n
7050-T7451	74	0.33	312.5	290	0.25
7050-T62	74	0.33	350	600	0.5

3.2. Numerical Simulation

Figure 4 illustrates the finite element model (FE model) using ABAQUS 6.14. Only half the structure is modeled, since the riveted lap joint is an axisymmetric structure along the three-rivet row. In an earlier study, a similar FE model was developed to study the residual stress and strain during riveting deformation processes [19]. The difference is that a displacement-controlled rivet installation process is substituted for the force-controlled method.

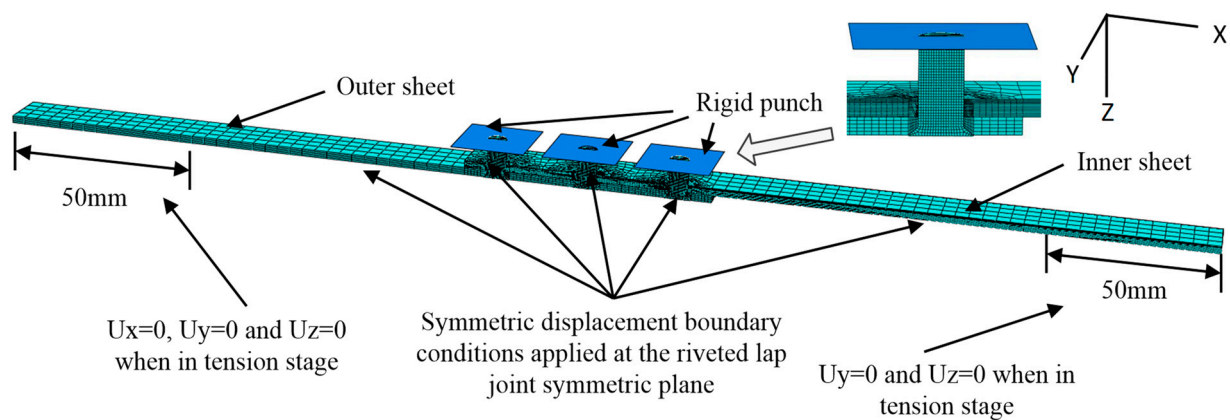


Figure 4. FE model of the riveted lap joint.

The FE model consists of three countersunk rivets, an outer sheet, an inner sheet and three rigid punches. The dimensions of the outer and inner sheets are $200 \times 26 \times 2$ mm. The minimum dimension ratio of the sheet and the rivet is 8 (larger than 6). The ratio value is large enough to eliminate the negligible effect on stress-free out boundaries [5,20]. The diameter and length of the rivet are 5mm and 11mm. The countersunk degree is 100° . The clearance between the hole wall and the rivet shank is 0.1 mm.

The FE model includes contacts between the rivet and sheets as well as the interface between the outer and inner sheets. The contact interaction is modeled with the Coulomb friction model. Additionally, a friction coefficient of 0.2 is specified for all the contact surfaces [11,21]. The sheets and countersunk rivet are built as deformable bodies. The punches are defined as rigid bodies. The deformable bodies are meshed by C3D8R. To balance the simulation's accuracy, model size and calculation cost, a typical mesh generation technology is applied [22,23]. The sheets are divided into several pieces. The mesh size in

the vicinity of the rivet hole is 0.1 mm, while the mesh size is 4 mm for the region far from the rivet hole. The whole model contains 128,808 elements.

Considering the symmetrical structure, the symmetrical displacement boundary conditions are applied at the symmetrical plane of the riveted lap joint. All degrees of freedom of the punches are constrained, except the Z direction. During the riveting process, there are no constraints applied at the far end of the outer and inner sheets. When in the tension stage, the far end of the outer sheet is fixed. Meanwhile, the far end of the inner sheet is constrained in the Y direction and Z direction. The tensile load acts on the far end of the inner sheet in the X direction.

Several analysis steps are defined. In the initial step, all the constraints on the rivets and punches are deactivated. Only the deformable bodies make contact with each other. Then, multiple load steps with their specific boundary conditions are sequentially introduced to the model:

In Step 1, squeezing displacement is applied to punches 1#, 2# and 3#, respectively. The riveting deformation process gradually occurs.

In Step 2, punches 1#, 2# and 3# are removed back to the origin.

In Step 3, tensile load (up to 150 MPa [24]) is applied to the riveted lap joint. The loading period is 2 seconds.

3.3. Experimental Test

The experiments aim to verify the validity of the theoretical analysis as well as the numerical simulation. Figure 5 illustrates the configuration of the test specimen. Two 7050-T7451 Al alloy sheets are riveted using three 7050-T62 Al alloy rivets. The sheet dimension is $200 \times 26 \times 2$ mm. The diameter of the rivet hole is 5.1 mm. The diameter and length of the rivet are 5 mm and 11 mm. The countersunk degree is 100° .

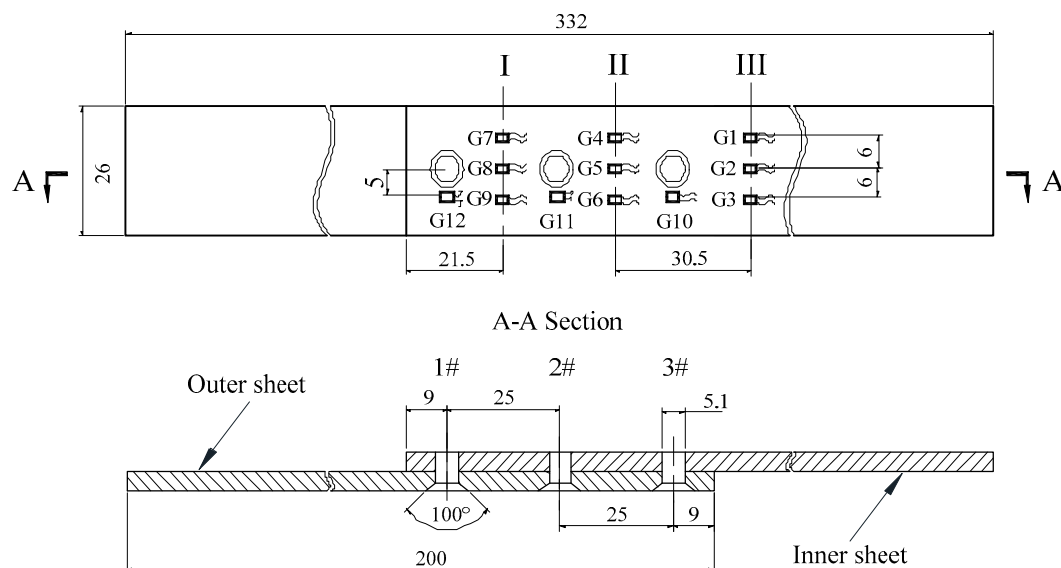


Figure 5. Overall configuration of the specimen (Unit: mm).

A tensile test is conducted using a multifunctional testing machine developed by Zhejiang University. Figure 6 illustrates the test device and its testing operation. The multifunctional testing machine is comprised of a reaction frame, hydraulic power system (YCQ-5 hydraulic jack and YZB50-2 \times 2 oil pump, Zhejiang University, Hangzhou, China), and strain sensor (RCT-21KN, Zhejiang University, Hangzhou, China, with sensitivity within 0.3%). Different squeezing displacement combinations have been designed. Each group contains five specimens.



Figure 6. Multi-function testing machine.

RCT-21KN Micro-strain gauges (Zhejiang University, Hangzhou, China) are employed to capture the strain variations during the tensile test. The dimension of these gauges is 2×1.5 mm. All gauges are installed on the inner sheet (the driven head side), as shown in Figure 5. Gauges (G1~G9) are mounted at different parts (I~III) to measure the longitudinal strain variations associated with tensile load distribution. The deformation magnitude of the interface between each part is measured by G10, G11 and G12.

Figure 7 illustrates the examples of different specimens after the tensile test. During the tensile test, tabs with dimensions of $50 \times 26 \times 2$ mm are fixed to the ends of each joint to eliminate the initial secondary bending moment. The specimen suffers a maximum remote stress of 146.2 MPa.

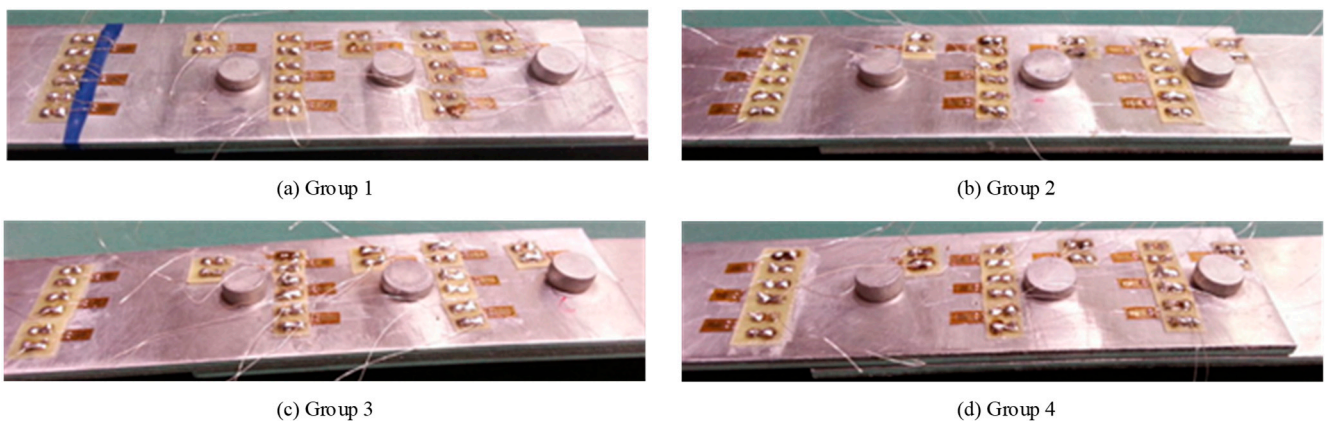


Figure 7. Experiment of riveted lap joint deformations after riveting. (a) Group 1. (b) Group 2. (c) Group 3. (d) Group 4.

4. Results and Discussion

The driven head dimension is usually considered as an indicator of riveting quality. According to the riveting criterion [17], the preferred height of a driven head is within 0.5–0.6 times of the original rivet diameter. Different squeezing displacements will produce different driven head dimensions. The relationship between squeezing displacement,

tensile load transmission as well as structural deformation is the main point in numerical simulations. Table 2 lists different squeezing displacement combinations.

Table 2. Vertical Offsets of Rivets.

Group	Squeezing Displacement/mm		
	1#	2#	3#
1	3.5	3.5	3.5
2	3.5	4.2	3.5
3	3.5	4.5	3.5
4	3.8	4.2	3.5

4.1. Numerical Simulation

The Von Mises stress is usually used to analyze the stress status [11]. Figure 8 illustrates the stress contours of the riveted lap joints after riveting and tension processes. As can be seen, the max stress of Rivet 2# is smaller than that of Rivets 1# and 3#. Additionally, at the same time, Rivet 2# in Group 1 carries minimum load compared with Rivet 2# in other groups. The stress concentration region of the outer rivets is highlighted in Group 1. The stresses of Rivet 2# in Group 2 and Group 4 become larger. Meanwhile, the stresses of Rivets 1# and 3# in Group 2 and Group 4 become smaller. The tension load distribution, in these cases, would tend to be more homogeneous. The stress of Rivet 2# in Group 3 is too big since the squeezing displacement of Rivet 2# is larger than any others. A new stress concentration region appears in Group 3.

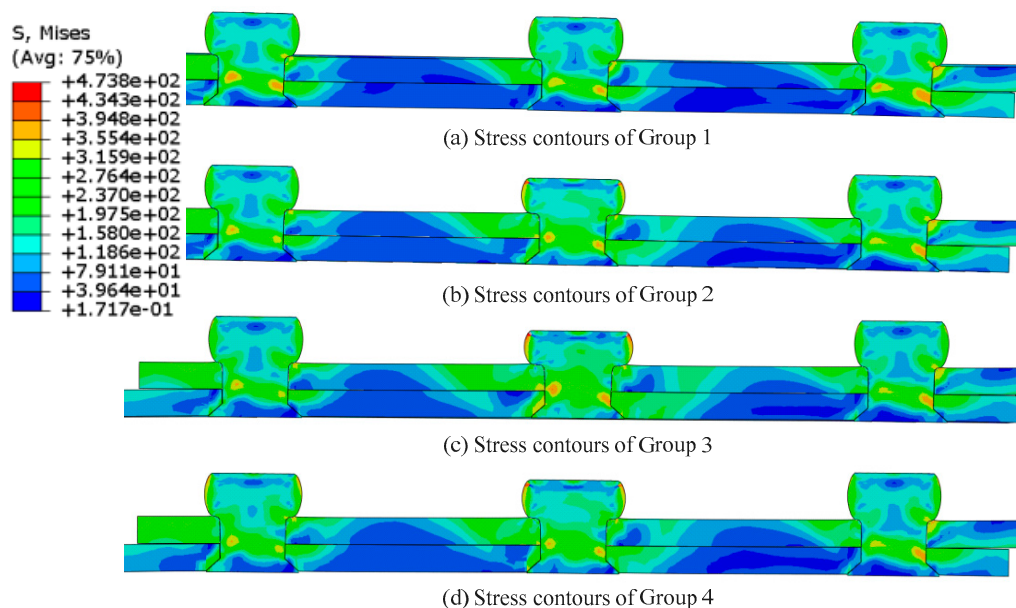


Figure 8. Stress contours of the riveted lap joints (Unit: MPa). (a) Stress contours of Group 1. (b) Stress contours of Group 2. (c) Stress contours of Group 3. (d) Stress contours of Group 4.

The purpose of this paper is to make tensile load distribution more homogeneous. As a result, the region of stress concentration is reduced correspondingly. The stress value will become smaller as well. Hence, according to analysis of stress contours, the squeezing displacements of Group 2 and Group 4 are relatively better.

Earlier studies indicated that the tensile load transmission is unequal for a normal multi-row riveted lap joint. Moreover, when the squeezing displacement becomes smaller, the distribution situation becomes worse. Figure 9 illustrates the tensile load distribution between three-row riveted lap joint.

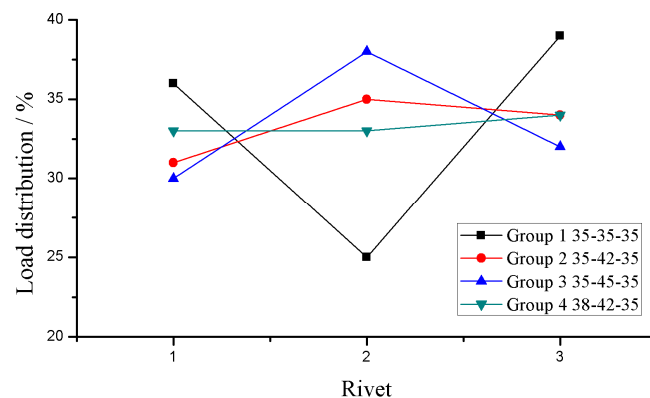


Figure 9. Tensile load transmission of a three-row riveted lap joint.

The situation of tensile load transmission varies with different squeezing displacement combinations. When the squeezing displacement of these three rivets is kept the same and remains smaller (Group 1), the tensile load distribution is quite inhomogeneous. The outer sides take a larger part of tensile load than the middle. When the squeezing displacement of Rivet 2# become larger, Rivet 2# will gradually transfer a larger part of tensile load. The results of Group 2 and Group 4 achieve a relatively more homogeneous tensile load distribution. In Group 4 especially, each rivet takes approximately one-third of the tensile load. However, Rivet 2# in Group 3 takes a great part of tensile load, since the squeezing displacement exceeds the normal value.

As analyzed before, for the inner sheet, the region most sensitive to tensile load is the interface of Part II and Part III around Rivet 3#. Since the interface has the minimum cross-sectional area with the largest tensile load, the interface becomes the most critical part of a riveted lap joint during the tensile stage. The deformation condition may be the worst. Figure 10 illustrates the structural deformation magnitude of the interface of Part II and Part III (G10 in Figure 5). The X axis is the loading period of the tensile load. The Y axis is the deformation magnitude.

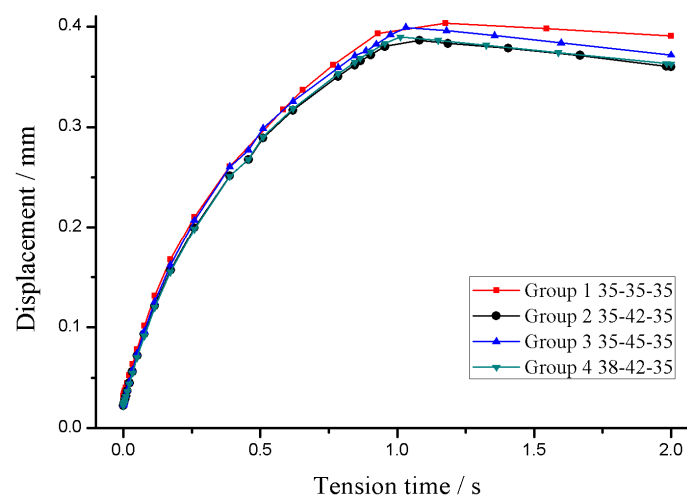


Figure 10. Deformation magnitude of the interface in the vicinity of Rivet 3# on inner sheet.

The magnitude is displayed in the form of measuring point displacement. The deformation of Group 1 is the worst due to its relatively small and equal squeezing displacement of the three rivets. The deformation of Group 2 and Group 4 achieves a better condition. Rivet 2# in Group 2 and Group 4 is installed with a larger squeezing displacement. The improvement of Group 3 is a little limited, since Rivet 2# in Group 3 is installed with the largest squeezing displacement. Clearly, the squeezing displacement combination has a

remarkable effect on the structural deformation of a riveted lap joint. Compared with Figure 9, when Rivet 2# takes a larger part of the tensile load, the structural deformation magnitude will be reduced as well.

4.2. Experimental Test and Discussion

The data of tensile load transmission as well as structural deformation can be easily and directly obtained with numerical simulation. However, the rivet and rivet hole would undergo a larger-scale plastic deformation during the riveting process. The outer and inner sheets form a tight junction with rivets. It is difficult to directly measure the data of tensile load transmission by experiments.

Therefore, except the driven head dimension, the tensile load distribution and structural deformation are measured by strain value, indirectly.

4.2.1. Comparison of Rivet Deformation

The comparison of driven head dimension gained from the numerical and experimental results is one of the useful methods to verify the validity of the FE model [11]. Table 3 summarizes the comparison results. Different squeezing displacement results in different driven head diameter. The relative difference of D/d is controlled within 5%. A good agreement is obtained. The numerical model has the ability to simulate the riveting process well.

Table 3. The Driven Head Deformation of D/d.

Squeezing Displacement/mm	Exp. D/d	FE D/d	Difference/%
3.5	1.38	1.42	2.90
3.8	1.44	1.5	4.17
4.2	1.56	1.6	2.56
4.5	1.64	1.68	2.44

4.2.2. Analysis of Tensile Load Distribution

Figure 11 illustrates the strain ratio under the effects of different squeezing displacements. The data are obtained from the micro-strain gauges mounted on the inner sheet. The X axis is the magnitude of tensile load. The Y axis is the strain ratio. As shown in Figure 2, the three-row riveted lap joint can be divided into four parts. Different parts suffer different proportions of tensile load. The proportion of tensile load transmitted by each part is closely related to the three rivets. The micro-strain gauges capture the strain variations of each part during the tensile test. The data shown in Figure 11 are the indirect index of tensile load transmission in actual experiments.

As mentioned before, strains of ε_{i1} , ε_{i2} , and ε_{i3} are the average strains of Sections 1–3, of which ε_{i3} is the total strain caused by tensile load $P = T_1 + T_2 + T_3$; ε_{i2} is the strain caused by $T_1 + T_2$; ε_{i1} is the strain caused by T_1 . In experiments, ε_{i1} is the average value of G7, G8 and G9; ε_{i2} is the average value of G4, G5 and G6. Additionally, ε_{i3} is the average value of G1, G2 and G3.

The strain ratios of $\varepsilon_{i2}/\varepsilon_{i3}$ and $\varepsilon_{i1}/\varepsilon_{i3}$ are regarded as indicators to evaluate the load distribution's homogeneity during tensile stage.

Obviously, in Group 2, the tensile load gradually transfers to Part I until the tensile load exceeds 20 MPa. When the tensile load is smaller than 20 MPa, strain ε_{i1} in Part I is close to zero. The load distribution in Group 3 is even worse. There are few load transmits to Part I when the tensile load is under 80 MPa. Strain ε_{i1} in Part I is close to zero. The tensile load finally transfers to Part II ($\varepsilon_{i2} \geq 0$) when the tensile load becomes larger than 50 MPa. This phenomenon can be explained, combined with Figure 9. In Group 2 and Group 3, Rivet 2# and Rivet 3# carry the vast majority of tensile load. Tensile load transfers part by part will become harder when load distribution condition become more inhomogeneous.

In contrast, for Group 1 and Group 4, the strain ratio of $\varepsilon_{i2} / \varepsilon_{i3}$ is nearly double the strain ratio of $\varepsilon_{i1} / \varepsilon_{i3}$, since the tensile load distribution becomes more homogeneous. Tensile load transfers part by part will become easier. In Group 4, in particular, the tensile load carried by the three rivets is approximately equal, $T_1 \approx T_2 \approx T_3 = P/3$. Hence, the load transferred by Part II ($T_1 + T_2$) is almost twice over the load delivered by Part I (T_1). The gap between the two strain ratio curves in Group 4 is larger than the gap in Group 1. This means the load distribution condition in Group 4 is better than in Group 1.

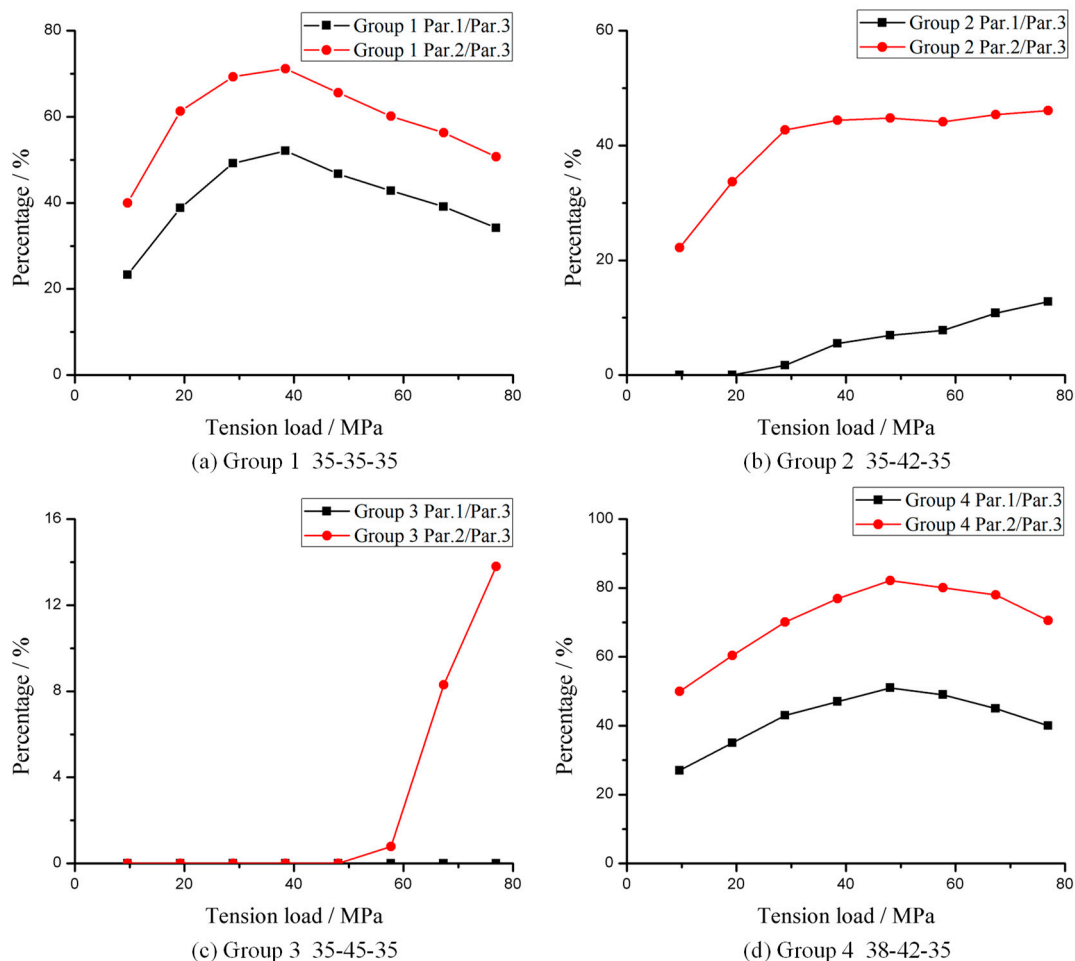


Figure 11. Curves of part strain ratio. (a) Group 1 35-35-35. (b) Group 2 35-42-35. (c) Group 3 35-45-35. (d) Group 4 38-42-35.

Both Figures 9 and 11 discuss the homogeneity of tensile load distribution. No matter simulation or experiment, Group 3 is the worst situation. Compared with Group 1 and Group 2, the condition of Group 4 is even better. This phenomenon may be caused by structural deformation. The squeezing displacement of the outer rivets remains the same in Group 2, while the situation in Group 4 is different. The special squeezing displacement of each rivet may have a significant impact on tensile load distribution. The tensile load distribution can be more homogeneous with an appropriate squeezing displacement combination.

4.2.3. Analysis of Structural Deformation

For the inner sheet, the region most sensitive to tensile load is the interface of Part II and Part III around Rivet 3#. The structural deformation at the interface around Rivet 3# is evaluated from the strain value of G10.

Figure 12 illustrates the strain value changing curve of G10. Since the rivet installation process will have some undesirable impacts on strain measurement, the strain value may be minus at the beginning when tensile load is transmitted to the corresponding section.

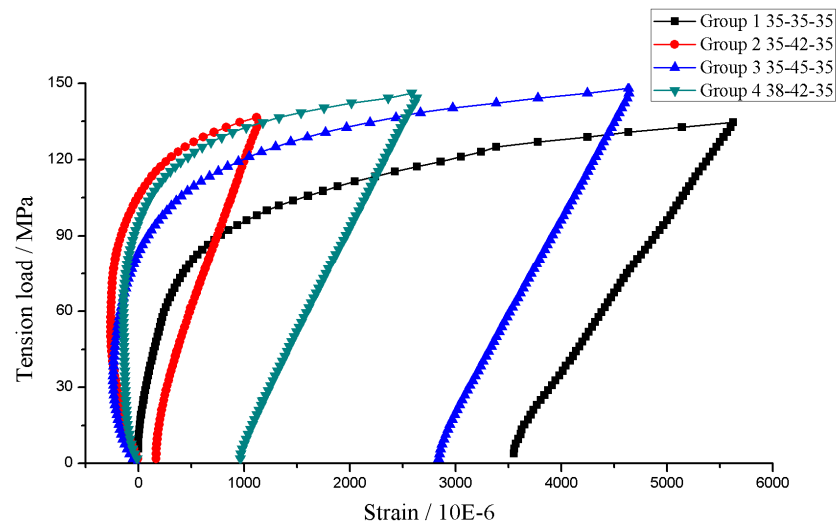


Figure 12. Strain value of Gauge 10.

The strain values of Group 2 and Group 4 are much smaller than other groups. The conditions of structural deformation in Group 2 and Group 4 are relatively better. When tensile load transmitted by the three rivets becomes nearly equal, the elongations of the outer and inner sheets between the end rows will be uniform. Group 1 and Group 3 undergo huge deformation.

Both Figures 10 and 12 discuss the condition of structural deformation. No matter simulation or experiment, Group 1 is the worst situation. The improvement of Group 3 is limited. The squeezing displacements of Group 2 and Group 4 are more desired. The structural deformation can be effectively controlled with an appropriate squeezing displacement combination.

5. Conclusions

The theoretical discussion introduces the internal moment model to account for the effect of the inhomogeneity of tensile load distribution. Numerical simulations and experimental tests are conducted. Four different squeezing displacement combinations are analyzed. A good agreement between theoretical analysis, numerical results and experimental tests is achieved.

The result of this paper indicates the squeezing displacement combination has a significant influence on the performance of a three-row riveted lap joint. An appropriate squeezing displacement combination can effectively make tensile load distribution more homogeneous. Each rivet can take approximately 33% tensile load. Structural deformation magnitude can be reduced as well. Compared with the worst situation, the max strain value at the region most sensitive to tensile load can reduce about 53.22–79.76%.

This study closely relates the squeezing displacement combination to tensile load distribution and structural deformation improvement. Squeezing displacement is not only an important riveting parameter, but is also easily controlled during the riveting process. The research of this work is of technological importance and is helpful to aircraft manufacturing practice.

Author Contributions: Conceptualization, C.L.; methodology, C.L. and Q.H.; software, C.L.; validation, C.L., Y.B. and Q.H.; formal analysis, Q.H.; investigation, Q.H.; resources, Y.B.; data curation, C.L.; writing—original draft preparation, C.L.; writing—review and editing, C.L.; visualization, C.L.; supervision, C.L.; project administration, C.L.; funding acquisition, C.L. All authors have read and agreed to the published version of the manuscript.

Funding: This research was funded by National Natural Science Foundation of China (No. 51905489) and the Research Foundation of Zhijiang College of Zhejiang University of Technology (No. 104190220).

Institutional Review Board Statement: Not applicable.

Informed Consent Statement: Not applicable.

Data Availability Statement: Data is contained within the article.

Acknowledgments: The authors would like to acknowledge Zhijiang College of Zhejiang University of Technology and Zhejiang University for technical and financial support to this research.

Conflicts of Interest: The authors declare no conflict of interest.

Nomenclature

ε_{i1}	The average strains of parts I in inner sheet.
ε_{i2}	The average strains of parts II in inner sheet.
ε_{i3}	The average strains of parts III in inner sheet.
ε_{o1}	The average strains of parts I in outer sheet.
ε_{o2}	The average strains of parts II in outer sheet.
ε_{o4}	The average strains of parts IV in outer sheet.
P	The tensile load.
T_1	The part of tensile carries by Rivet 1#.
T_2	The part of tensile carries by Rivet 2#.
T_3	The part of tensile carries by Rivet 3#.
M_1	The internal moment at Rivet 1#.
M_2	The internal moment at Rivet 2#.
M_3	The internal moment at Rivet 3#.
ε	The true strain.
$\sigma(\varepsilon)$	The true stress.
A	Material constant.
B	Material constant.
n	Material hardening behavior.
D	The diameter of driven head.
d	The original diameter of rivet.

References

1. Wang, M.; Xue, S.D.; Chen, W.L.; Chen, L.; Jiang, H.Y. One-side pressed burrless drilling technology for aircraft automatic assembly. *Aeronaut. Manuf. Technol.* **2011**, *9*, 26–29.
2. Skorupa, A.; Skorupa, M.; Machniewicz, T.; Korb, A. Fatigue crack location and fatigue life for riveted lap joints in aircraft fuselage. *Int. J. Fatigue* **2014**, *58*, 209–217. [[CrossRef](#)]
3. Lei, C.Y.; Bi, Y.B.; Li, J.X. Continuous Numerical Analysis of Slug Rivet Installation Process Using Parameterized Modeling Method. *Coatings* **2021**, *11*, 189. [[CrossRef](#)]
4. Huang, W.; Wang, T.J.; Garbatov, Y.; Soares, C.G. Fatigue reliability assessment of riveted lap joint of aircraft structures. *Int. J. Fatigue* **2012**, *43*, 54–61. [[CrossRef](#)]
5. Muller, R.P. *An Experimental and Analytical Investigation on the Fatigue Behavior of Fuselage Riveted Lap Joints*; Delft University of Technology: Delft, The Netherlands, 1995.
6. Osama, K.B.; Graeme, F.E. A numerical model for analysis of riveted splice joints accounting for secondary bending and plates/rivet interaction. *Thin Wall Struct.* **2007**, *45*, 251–258.
7. Naarayan, S.S.; Kumar, P.; Chandra, S. Implication of unequal rivet load distribution in the failures and damage tolerant design of metal and composite civil aircraft riveted lap joints. *Eng. Fail. Anal.* **2009**, *16*, 2255–2273. [[CrossRef](#)]
8. Rijk, J.J. *Stress Analysis of Fatigue Cracks in Mechanically Fastened Joints*; Delft University of Technology: Delft, The Netherlands, 2005.
9. Aman, F.; Cheraghi, S.H.; Krishnan, K.K.; Lankarani, H. Study of the impact of riveting sequence, rivet pitch, and gap between sheets on the quality of riveted lap joints using finite element method. *Int. J. Adv. Manuf. Technol.* **2013**, *67*, 545–562. [[CrossRef](#)]

10. Park, C.Y.; Grandt, J.A. Effect of load transfer on the cracking behavior at countersunk fastener hole. *Int. J. Fatigue* **2007**, *29*, 146–157. [[CrossRef](#)]
11. Atre, A. *A Finite Element and Experimental Investigation on the Fatigue of Riveted Lap Joints in Aircraft Applications*; Georgia Institute of Technology: Atlanta, GA, USA, 2006.
12. Jiang, C.P.; Zhang, X. An analytical method of pin load computations for joints with multi-fasteners. *Acta Aeronaut. Astronaut. Sin.* **1994**, *15*, 310–317.
13. Liu, X.D.; Li, Y.Z.; Shu, H. Experimental and numerical study on the pin-load distribution of multiple-bolted joints. *Acta Mater. Compos. Sin.* **2013**, *30*, 210–217.
14. Abdelal, G.F.; Georgiou, G.; Cooper, J.; Robotham, A.; Levers, A.; Lunt, P. Numerical and Experimental Investigation of Aircraft Panel Deformations During Riveting Process. *J. Manuf. Sci. E.T. ASME* **2015**, *137*, 1–11. [[CrossRef](#)]
15. Yuan, X.; Yue, Z.F.; Yan, W.Z.; Wen, S.F.; Li, L. Experimental and analytical investigation of fatigue and fracture behaviors for scarfed lap riveted lap joints with different lap angle. *Eng. Fail. Anal.* **2013**, *33*, 505–516. [[CrossRef](#)]
16. Rijck, J.J.; Homan, J.J.; Schijve, J.; Benedictus, R. The driven head dimensions as an indication of the fatigue performance of aircraft lap joints. *Int. J. Fatigue* **2007**, *29*, 2208–2218.
17. Reithmaier, L.; Sterkenburg, R. *Standard Aircraft Handbook for Mechanics and Technicians*, 7th ed.; McGraw-Hill Education: New York, NY, USA, 2014.
18. Dai, S.L.; Zhang, K. *Advanced Aeronautical Aluminum Alloy Materials Technology and Application*; National Defence Industry Press: Beijing, China, 2012.
19. Li, G.; Shi, G.Q.; Bellinger, N.C. Residual Stress/Strain in Three-Row, Countersunk, Riveted Lap Joint. *AIAA ASME ASCE AHS ASC 47th Struct. Struct. Dyn. Mater. Conf.* **2007**, *44*, 1275–1285. [[CrossRef](#)]
20. Godwin, E.W.; Matthews, F.L. A review of the strength of joints in fiber-reinforced plastic mechanically fastened joints. *Composites* **1980**, *11*, 155–160. [[CrossRef](#)]
21. Szolwinski, M.P. *The Mechanics and Tribology of Fretting Fatigue with Application to Riveted Lap Joint*; School of Aeronautics and Astronautics, Purdue University: West Lafayette, IN, USA, 1998.
22. Blanchot, V.; Daidie, A. Riveted assembly modeling: Study and numerical characterization of a riveting process. *J. Mater Process Tech.* **2006**, *43*, 592–599.
23. Lei, C.Y.; Bi, Y.B.; Li, J.X.; Ke, Y.L. Experiment and numerical simulations of a slug rivet installation process based on different modeling methods. *Int. J. Adv. Manuf. Tech.* **2018**, *97*, 1481–1496. [[CrossRef](#)]
24. De Castro, P.M.S.T.; de Matos, P.F.P.; Moreira, P.M.G.P.; de Silva, L.F.M. An overview on fatigue analysis of aeronautical structural details: Open hole, single rivet lap-joint, and lap-joint panel. *Mat. Sci. Eng. A Struct.* **2007**, *468–470*, 144–157. [[CrossRef](#)]